Investigations on the Properties of Nanostructured Mg-Doped Sn_2S_3 Thin Films towards Photovoltaic Applications

S. Joshua Gnanamuthu[a], I. Kartharinal Punithavathy[a], S. Johnson Jeyakumar[a], P.C. Jobe Prabhakar[a], K. Parasuraman[b], V.S. Nagarethinam[c], K. Usharani[c] and A.R. Balu[c,*]

[a]Department of Physics, TBML College, Poraiyar, Tamilnadu, India
[b]Department of Physics, Poompukar Arts College, Melaiyur, Tamilnadu, India
[c]Department of Physics, AVVM Sri Pushpam College, Poondi, Tamilnadu, India

(Received March 27, 2016; in final form November 25, 2017)

This paper reports the synthesis, crystal structure, surface morphology, optical and electrical properties of Mg-doped Sn_2S_3 thin films deposited by spray pyrolysis technique. All the films exhibit orthorhombic crystal structure with a (211) preferential orientation. Crystallite size calculations based on the Debye–Scherrer formula indicated that the Sn_2S_3 crystallite size increases with Mg content from 27.97 nm to 33.58 nm. Scanning electron microscopy images showed that all the films were very smooth composed of nanoneedle and nanoplate shaped grains. The band gap energy of the films exhibits a blue shift from 1.94 eV to 2.09 eV with increase in Mg concentration. Resistivity values of the undoped and Mg-doped Sn_2S_3 films were found to be in the order of 0.1 Ωcm. From the obtained results it is observed that the Sn_2S_3 film coated with 2 wt% Mg concentration exhibits better physical properties.

DOI: 10.12693/APhysPolA.133.15

PACS/topics: 61.05.cp, 77.84.Bw, 78.66.Jg, 68.55.Ln, 78.20.Ci, 73.61.Jc

1. Introduction

Tin sulphide, a chalcogenide compound belonging to a family of IV–VI semiconductors have attracted attention in recent decades due to its numerous applications. Its band gap varies in the range of 0.8–3.5 eV [1, 2] which make it suitable as an absorber or window layer in photovoltaic solar cells. Tin sulphide has three main phases of which SnS_2 and SnS exhibit layered structure whereas Sn_2S_3 exhibit ribbon-like structure [3]. Sn_2S_3, a material with electron lone pairs is a mixed valence Sn compound which crystallizes in orthorhombic crystal structure [4]. Sn_2S_3 is a direct forbidden semiconductor with a band gap of 0.95 eV and high anisotropic conduction [5], which makes it suitable as *p–n* or *p–i–n* structures in photovoltaic applications [6]. Sn_2S_3 could also be used to prepare near-lattice-matched hetero junctions such as Sn_2S_3/CdTe, Sn_2S_3/GaSb, Sn_2S_3/AlSb, etc, for applications in the detection and generation of infrared radiation [7].

Due to the existence of numerous particle boundaries, Sn_2S_3 films have low electron-transport efficiency, which would result in easy recombination of electrons and holes thereby limiting the efficiencies of Sn_2S_3 based solar cells. It has been proposed recently that in 3D nanostructured networks comprised of semiconductor nanorods, nanotubes or nanowires high electron transport rate could be achieved, as these networks provide direct conduction pathways for rapid collection of photo-generated electrons [8]. In photoelectric conversion, these 3D networks can enhance relaxation light harvesting by multiple scattering thereby increasing the conversion efficiency [9]. Sn_2S_3 is one such material which exhibit 3D nanostructured network depending on the preparation conditions.

Sn_2S_3 thin films have been prepared earlier by various techniques such as spray pyrolysis [10], chemical bath deposition [11], potentiostatic electrodeposition [12], etc. Among these techniques, spray pyrolysis is a promising technique for preparing semiconducting thin films suitable for energy conversion applications. The conductivity and carrier concentration of Sn_2S_3 films deposited by spray pyrolysis technique have been estimated about 4.35×10^{-3} $(\Omega\text{cm})^{-1}$ and 9.4×10^{14} cm^{-3}, respectively. It has been reported earlier that the resistivity of Sn_2S_3 is affected by the increased number of grains possessed by it [13]. Also Sn_2S_3 films with tin vacancies show *p*-type conductivity, while the films with sulphur vacancies show *n*-type conductivity [14]. In Sn_2S_3, carrier type might be subject to change as its carrier concentration is sensitive to the growth or annealing conditions as the formation energies of the tin and sulphur vacancy defects are close in energy.

In photovoltaic applications, mixed type of Sn_2S_3 would be detrimental to its transport properties which would lower the device performance. Therefore, in order to improve the photovoltaic device performance, single phase Sn_2S_3 is essential which can be achieved by controlling the Sn and S vacancies. However, the for-

*corresponding author; e-mail: arbalu757@gmail.com

mation of p-type Sn_2S_3 is very difficult because of strong self-compensation effect due to sulphur vacancies and the depth of the acceptor level. To form a single phase Sn_2S_3 of p-type, it is essential to control the self-compensation effect due to sulphur vacancies which can be achieved through doping.

Magnesium is a transition metal element belonging to $P63/mmc$ space group. Mg^{2+} has an ionic radius of 0.72 Å which is small compared to that of Sn^{2+} (0.93 Å). Therefore, doping of Mg in Sn_2S_3 permits its band gap to be tailored and also Mg doped Sn_2S_3 leaves the lattice constants almost invariant due to the high solid solubility of MgS in Sn_2S_3. Also Mg metal based sulphide thin films exhibit p-type conductivity. Therefore, it is expected that when MgS is alloyed with Sn_2S_3, it may be possible to form a single phase of Sn_2S_3 with p-type. Motivated by this fact, in this work Mg-doped Sn_2S_3 films were prepared by spray pyrolysis technique with different concentrations of Mg (0, 1, 2, and 3 wt%) and the effect of Mg doping on the properties of Sn_2S_3 films was investigated and the results are reported here.

2. Experimental details

Sn_2S_3 films were deposited by spray pyrolysis technique using tin(II) chloride, ($SnCl_2{\cdot}H_2O$)(0.02 M) and thiourea $CS(NH_2)_2$ (0.02 M) as precursor salts. First $SnCl_2$ is dissolved in a mixture of HCl and deionized water in the volume ratio of 1:5 (in total 30 ml volume) while thiourea was added to this solution and stirred well for 30 min. To achieve Mg doping, $MgCl_2$ is used as the precursor salt. Mg concentration is varied in the starting solution as 0, 1, 2, and 3 wt%. The resultant solution was sprayed on glass substrates kept at 400 °C, with help of compressed air at a flow rate of 6 ml/min. The distance between the spray nozzle and the heater was kept approximately at 28 cm. The thicknesses of the Sn_2S_3 films coated with 0, 1, 2 and 3 wt% Mg concentrations measured by Profilometer (SJ-301) were found to be equal to 240, 252, 269 and 256 nm respectively. X-ray diffraction (XRD) patterns of the films were obtained with the help of X-ray diffractometer (PANalytical — PW 340/60 X'pert PRO) with Cu K_α ($\lambda = 1.5406$ Å) radiation as X-ray source. The surface morphology of the films was studied using scanning electron microscope (HITACHI S — 3000H). Optical studies were performed using a UV-Vis-NIR double beam spectrophotometer (LAMDA — 35) in the wavelength range 300–1100 nm. Electrical and photoluminescence studies were carried out using a two point probe setup and Varian Cary Eclipse Fluorescence spectrophotometer, respectively.

3. Results and discussion

3.1. XRD analysis

Figure 1 shows the XRD patterns of Mg-doped Sn_2S_3 thin films coated with 0, 1, 2 and 3 wt% Mg concentrations. All the films exhibit a well defined peak at about 31.71° and a weak peak at 66.26° corresponding to the (211) and (422) planes of orthorhombic structure (JCPDS card No. 75-2183). Besides these peaks, no extra peaks corresponding to any phase of tin sulphide were observed confirming that the as deposited films were of Sn_2S_3 phase only. It is observed that the peak intensity of the (211) plane increased with increase of Mg content attaining a maximum value for the film coated with 2 wt% doping concentration indicating better crystallinity of this film. The crystallite size D of the Mg-doped Sn_2S_3 films was calculated from the Scherrer formula [15]:

$$D = \frac{0.9\lambda}{\beta \cos\theta}, \tag{3.1}$$

where λ is the wavelength of the X-ray (1.5406 Å), β is the full width at half maximum and θ is the Bragg angle. The calculated crystallite values increases with doping concentration and the Sn_2S_3 film coated with 2 wt% Mg concentration is found to have maximum crystallite value of 33.58 nm confirming its improved crystallinity.

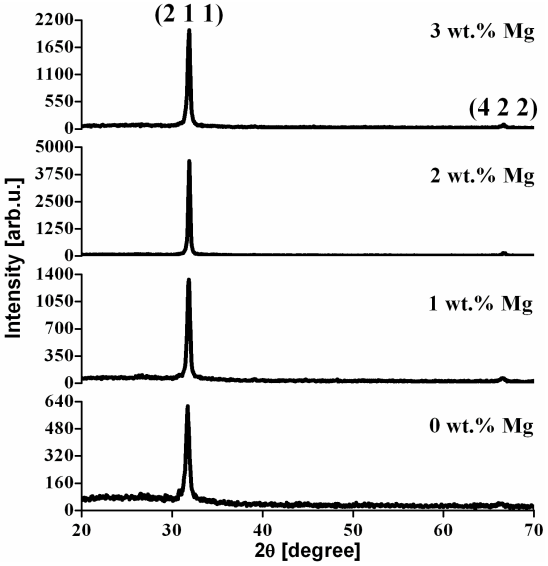

Fig. 1. XRD patterns of Mg-doped Sn_2S_3 thin films.

TABLE I

Structural parameters of Mg doped Sn_2S_3 thin films for given Mg doping concentration.

Mg [wt%]	$2\theta_{(2111)}$	D [nm]	ε $\times 10^{-3}$	Lattice parameters [Å]		
				a	b	c
0	31.706°	27.97	1.2390	5.641	15.622	5.642
1	31.856°	30.82	1.1244	5.619	15.551	5.658
2	31.892°	33.58	1.0320	5.612	15.533	5.652
3	31.880°	32.88	1.0539	5.614	15.538	5.654

It is observed from the XRD patterns that the 2θ value of the (211) plane of the Sn_2S_3 films shifts towards higher Bragg angle (Table I) with increase in Mg concentration

inferring a contraction in their lattice volumes. The calculated lattice parameter values of the Mg-doped Sn_2S_3 thin films decreases with increase in Mg concentration which infer that Mg^{2+} ions have substitutionally replaced Sn^{2+} ions in the host lattice. This inference is arrived as the ionic radius of Mg^{2+} (0.72 Å) is smaller than Sn^{2+} (0.93 Å).

The strain in the film was calculated using the relation [16]:

$$\varepsilon = \frac{\beta \cos\theta}{4}. \tag{3.2}$$

The obtained values decreases with increase in Mg concentration and the film coated with 2 wt% Mg concentration exhibited a low value of strain confirming its improved crystallinity.

3.2. SEM analysis

Figure 2a–d shows the SEM images of Mg-doped Sn_2S_3 thin films. It is observed that the surface of pure Sn_2S_3 film is smooth and dense composed of nanoneedle shaped grains (Fig. 2a). For 1 wt% Mg dopant, the film surface seems to be tightly packed with a mixture of needle shaped and plate-like grains (Fig. 2b). As the Mg concentration is increased further, the surface gets modified with equally sized nanoneedles for the film coated with 2 wt% Mg concentration (Fig. 2c). With further increase in Mg concentration, the surface gets modified with equally sized plate like grains along with few nanoneedles for the film coated with 3 wt% Mg concentration (Fig. 2d). These results infer that Mg doping strongly influences the surface morphology of pure Sn_2S_3 film and it is observed that the film coated with 2 wt% Mg concentration exhibits better morphology supporting the results obtained in XRD analysis.

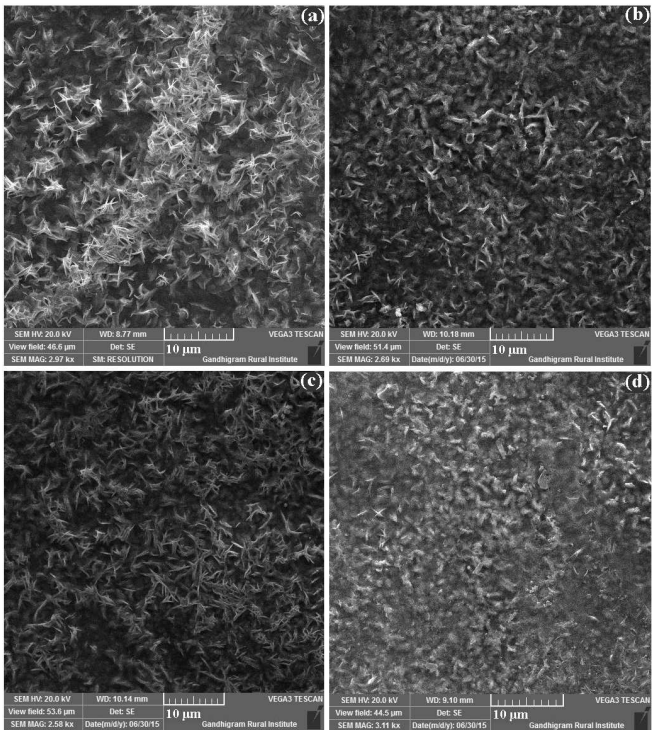

Fig. 2. SEM images of Mg-doped Sn_2S_3 thin films.

3.3. Electrical studies

The electrical resistivity values of the films measured by two point probe setup are compiled in Table II. The resistivity values of the films are found to be in the range of 10^{-1} Ωcm. The resistivity range obtained here exactly matched with earlier reports [17]. It can be observed that film resistivity decreases with increase in Mg concentration, attaining a minimum value of 1.13×10^{-1} Ωcm for the film coated with 2 wt% Mg concentration. The decreased resistivity values observed with Mg doping might be due to increased crystallite size or decreased lattice strain and improved crystallinity. The reduction in resistivity with Mg doping might also be due to increased carrier concentration which might have occurred due to substitutional incorporation of Mg^{2+} ions into the host lattice.

TABLE II

Optical parameters and electrical resistivity values of Mg-doped Sn_2S_3 thin films for given Mg doping concentration.

Mg [wt%]	E_g [eV]	$E_u \times 10^{-2}$ [eV]	$\rho \times 10^{-1}$ [Ωcm]
0	1.94	3.28	5.81
1	2	3.19	3.69
2	2.09	2.97	1.13
3	2.04	3.10	2.62

3.4. Optical studies

Figure 3 shows the optical transmittance spectra of undoped and Mg-doped Sn_2S_3 thin films recorded in the wavelength range of 300–1100 nm. The average transmittance of the Mg-doped Sn_2S_3 films decreases with increase in the Mg content which may be due to increased absorption by free carriers [18]. It is also observed that the absorption edge of the doped films shift towards lower wavelength side which indirectly indicate an increment in their band gap values. In semiconductor materials, optical transitions take place by direct and indirect transitions. The fundamental absorption, which corresponds to electron excitation from the valence band to conduction band, can be used to determine the optical band gap E_g of Mg-doped Sn_2S_3 films. The band gap values can be obtained from the optical absorption spectra by the relation [19]:

$$\alpha h\upsilon = A(h\upsilon - E_g)^n, \tag{3.3}$$

where α is the absorption coefficient, $h\upsilon$ is the photon energy, n assumes the values 1/2, 2, 3/2, and 3 for allowed direct, allowed indirect, forbidden direct, and forbidden indirect transitions, respectively. A is a constant related to the extent of band tailing. The band gap values were determined by extrapolating the linear portion

of the plots of $(\alpha h\upsilon)^2$ versus $h\upsilon$ (Fig. 4) until they intercept the $h\upsilon$ axis at $\alpha = 0$. The E_g values of the Mg-doped Sn_2S_3 films are listed in Table II. It is observed that the undoped film has a band gap of 1.94 eV which exactly matches with the value reported by Guneri et al. [11] for Sn_2S_3 films deposited by chemical bath technique. As can be seen from Table II, the E_g values of the doped films were found to be blue shifted, which can be attributed to the Burstein–Moss (BM) effect. According to BM effect, band gap increases as the dopant elements lead to an increase of electrons in the conduction band shifting the Fermi level. However, the substitution of Mg^{2+} in the Sn^{2+} sites do not offer any free carriers due to the covalence of these ions. Hence, it can be concluded that the increase in the band gap observed here is not associated with the BM effect and may be due to other factors which can be explained as follows: when Mg is alloyed with Sn_2S_3, as MgS has higher band gap energy (4.65 eV) than Sn_2S_3 (0.95 eV), the increase in the Mg concentration gradually increases the band gap which infers that the contribution of Mg-3s state becomes dominant at the bottom of the conduction band which broadens the optical band gap by heightening the bottom of the conduction band [20].

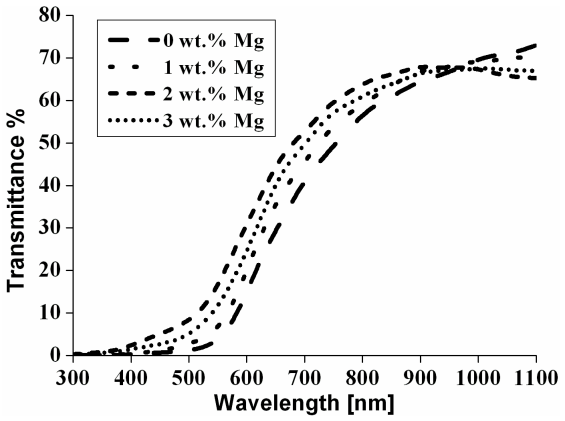

Fig. 3. Transmittance spectra of Mg-doped Sn_2S_3 thin films.

The Urbach tail, the width of the localized states available in the band gap region of thin films, affects their band gap structure and transitions [21]. The Urbach tail of the Mg-doped Sn_2S_3 thin films was determined by the relation [22]:

$$\alpha = \alpha_0 \exp\left(E/E_u\right), \tag{3.4}$$

where E is the photon energy, α_0 is constant and E_u is the Urbach energy which refers to the width of the exponential absorption edge. The E_u values of the Mg-doped Sn_2S_3 thin films were calculated from the slopes of the plots between $\ln(\alpha)$ vs. $h\upsilon$ (Fig. 5), and the obtained E_u values increase in Mg concentration supports for the improved crystallinity of the doped films, which means that there are only minimum number of defects in the Sn_2S_3 film structure even after doped with Mg. It is

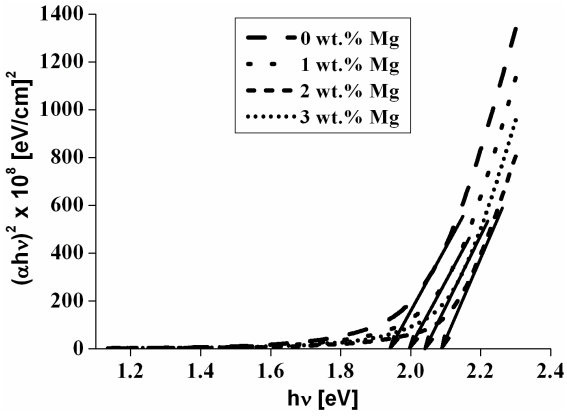

Fig. 4. Plots of $(\alpha h\nu)^2$ vs. $h\nu$ of Mg-doped Sn_2S_3 thin films.

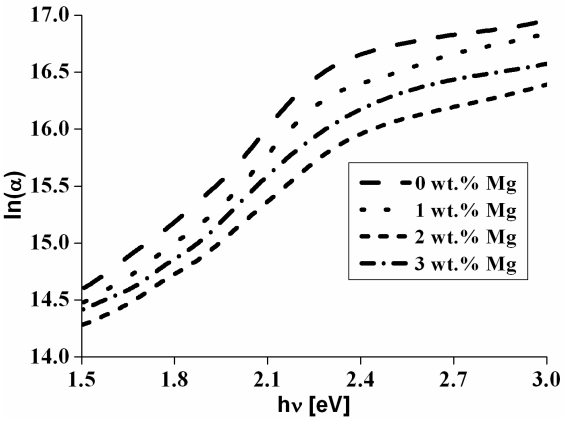

Fig. 5. Plots of $\ln(\alpha)$ vs. $h\nu$ of Mg-doped Sn_2S_3 thin films.

also observed that both E_g and E_u values vary in opposite ways. The low value of E_u observed for the Sn_2S_3 film coated with 2 wt% Mg concentration for which E_g is maximum confirm the minimization of defects in this film which favours for its improved crystalline nature.

3.5. PL studies

Photoluminescence (PL) spectrum provides information on the optically active defects and relaxation pathways of excited states. Information regarding the point defects present in thin films such as vacancies, interstitials and impurities can be obtained from PL studies [23]. Figure 6 displays the PL spectra of the undoped and Mg-doped Sn_2S_3 (Mg doping levels: 2 and 3 wt%) thin films, excited at $\lambda = 400$ nm. It is observed that all the films exhibit emission peaks at 485 nm (2.56 eV), 544 nm (2.28 eV) and 608 nm (2.04 eV). The peak at 485 nm can be attributed to the transitions of trapped electrons from donor levels to the valence band which can be assigned to defect states, probably S vacancy states [24]. The green band emission observed at 2.28 eV has been originated from the transition of the increased

V_s donors to recombine with S interstitials (I_s) acceptors in the valence band [25]. The yellow band emission observed at 2.04 eV is caused by a donor–acceptor pair [26]. Ahmad-Bitar [27] reported a similar band for CdS thin films which they attributed to recombination via surface localized states, a transition from cadmium interstitial (I_{Cd}) to valence band, and the transition from interstitial cadmium–cadmium vacancy complex $I^{+}_{\mathrm{Cd}}-V^{-}_{\mathrm{Cd}}$ which acts as a donor to an acceptor level.

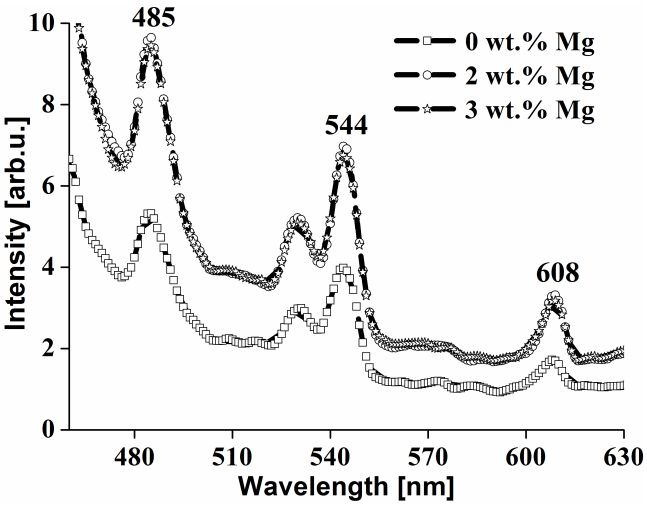

Fig. 6. PL spectra of Mg-doped Sn_2S_3 thin films.

4. Conclusion

Nanostructured pure and Mg-doped Sn_2S_3 thin films were prepared by spray pyrolysis technique. The effect of Mg doping on the structural, morphological, optical and electrical properties of Sn_2S_3 films were investigated. XRD studies revealed that all the films exhibited orthorhombic structure with a preferential orientation along the (211) plane. The 2θ angle of the (211) peak was found to be shifted towards higher Bragg angle with increasing Mg content in the films. Crystallite size increased from 27.97 nm to 33.58 nm with increase in Mg concentration. The presence of nano needles in the films is evinced from the SEM images. Optical band gap was blue shifted with doping. Urbach energy decreased with increasing Mg concentration confirming the decrement in the disorderliness of the films with doping. Film coated with 2 wt% Mg concentration exhibited a minimum resistivity of 1.13×10^{-1} Ωcm. From the obtained results, it was confirmed that the Sn_2S_3 film coated with 2 wt% Mg concentration exhibited better physical properties which make them suitable for photovoltaic applications.

References

[1] S.K. Panda, A. Antonakos, E. Liarokapis, S. Bhattacharya, S. Chaudhuri, *Mater. Res. Bull.* **42**, 576 (2007).

[2] S. Acharya, O.N. Srivastava, *Phys. Status Solidi A* **65**, 717 (1981).

[3] T. Jiang, G.A. Ozin, *J. Mater. Chem.* **8**, 1099 (1998).

[4] W. Saito, K. Hayashi, H. Nagai, Y. Miyazaki, *Jpn. J. Appl. Phys.* **56**, 061201 (2017).

[5] D.J. Singh, *Appl. Phys. Lett.* **109**, 032102 (2016).

[6] J.J. Lofersky, *J. Appl. Phys.* **27**, 777 (1956).

[7] S. Lopez, S. Granados, A. Ortiz, *Semicond. Sci. Technol.* **11**, 433 (1996).

[8] H.M. Cheng, W.H. Chiu, C.K. Lee, S.Y. Tsai, W.F. Hsieh, *J. Phys. Chem. C* **112**, 16359 (2008).

[9] S. Matsushita, O. Suavet, H. Hashiba, *Electrochem. Acta* **55**, 2398 (2010).

[10] D. Prabha, S. Ilangovan, V.S. Nagarethinam, A.R. Balu, *Mater. Res. Innov.* **20**, 301 (2015).

[11] E. Guneri, F. Gode, B. Boyarbay, C. Gumus, *Mater. Res. Bull.* **47**, 3738 (2012).

[12] B. Chen, X. Xu, F. Wang, J. Liu, J. Ji, *Mater. Lett.* **65**, 400 (2011).

[13] M. Khadraoui, N. Bonramdane, C. Mathieu, A. Bouzidi, R. Miloua, Z. Kebbab, *Solid State Commun.* **150**, 297 (2009).

[14] J.J. Scragg, P.J. Dale, L.M. Peter, G. Zoppi, I. Forbes, *Physica Status Solidi B* **245**, 1772 (2008).

[15] M. Anbarasi, V.S. Nagarethinam, A.R. Balu, *Mater. Sci. Poland* **32**, 652 (2014).

[16] K. Usharani, A.R. Balu, *Acta Metall. Sinica (Eng. Lett.)* **28**, 64 (2014).

[17] L.A. Burton, D. Colombara, R.D. Abellon, F.C. Grazema, L.M. Peter, T.J. Savenjie, G. Dennler, A. Walsh, *Chem. Mater.* **25**, 4908 (2013).

[18] X. Wu, T.J. Coutts, W.P. Mulligan, *J. Vac. Sci. Technol. A* **15**, 1057 (1997).

[19] K. Usharani, A.R. Balu, V.S. Nagarethinam, M. Suganya, *Progr. Nat. Sci. Mater. Int.* **25**, 251 (2015).

[20] S. Gowrishankar, L. Balakrishnan, N. Gopalakrishnan, *Ceram. Int.* **40**, 2135 (2014).

[21] G.D. Cody, *J. Non-Cryst. Solids* **141**, 3 (1992).

[22] F. Urbach, *Phys. Rev.* **92**, 1324 (1953).

[23] T. Sivaraman, A.R. Balu, V.S. Nagarethinam, *Mater. Sci. Semicond. Proc.* **27**, 915 (2014).

[24] T. Sivaraman, V.S. Nagarethinam, A.R. Balu, *Surf. Eng.* **32**, 596 (2016).

[25] B.S. Moon, J.H. Lee, H. Jung, *Thin Solid Films* **511-512**, 299 (2006).

[26] L. Wan, Z. Bai, Z. Hou, D. Wang, H. Sun, I. Xiong, *Thin Solid Films* **518**, 6858 (2010).

[27] R.N. Ahmad-Bitar, *Renew. En.* **19**, 579 (2000).